Guidelines for standardization of bioprinting: a systematic study of process parameters and their effect on bioprinted structures

Guidelines for standardization of bioprinting: A systematic study of process parameters and their effect on bioprinted structures

*Matti Kesti, Philipp Fisch, Marco Pensalfini, Edoardo Mazza, Marcy Zenobi-Wong**

M. Kesti, P. Fisch, Prof. M. Zenobi-Wong
Cartilage Engineering + Regeneration, Institute for Biomechanics, ETH Zürich, 8093 Zürich, Switzerland

M. Pensalfini, Prof. E. Mazza
Experimental continuum mechanics, Institute for Mechanical Systems, ETH Zürich, 8092 Zürich, Switzerland
Swiss Federal Laboratories for Materials Science and Technology, EMPA, 8600 Dübendorf, Switzerland

ETH Zürich
Otto-Stern-Weg 7, HPL J22
8093 Zürich
Switzerland
E-mail: marcy.zenobi@hest.ethz.ch
Phone: +41 44 632 50 89

Abstract

Biofabrication techniques including three-dimensional bioprinting could be used one day to fabricate living, patient-specific tissues and organs for use in regenerative medicine. Compared to traditional casting and molding methods, bioprinted structures can be much more complex, containing for example multiple materials and cell types in controlled spatial arrangement, engineered porosity, reinforcement structures and gradients in mechanical properties. With this complexity and increased function, however, comes the necessity to develop guidelines to standardize the bioprinting process, so printed grafts can safely enter the clinics. The bioink material must firstly fulfill requirements for biocompatibility and flow. Secondly, it is important to understand how process parameters affect the final mechanical properties of the printed graft. Using a gellan-alginate physically crosslinked bioink as an example, we show shear thinning and shear recovery properties which allow good printing resolution. Printed tensile specimens were used to systematically assess effect of line spacing, printing direction and crosslinking conditions. This standardized testing allowed direct comparison between this bioink and three commercially-available products. Bioprinting is a promising, yet complex fabrication method whose outcome is sensitive to a range of process parameters. This study provides the foundation for highly needed best practice guidelines for reproducible and safe bioprinted grafts.

Key words: Additive manufacturing; biofabrication; extrusion bioprinting; standards; mechanical testing; hydrogel

Introduction

Bioprinting is a fabrication technique which has been developing over the past 20 years, however, there are no commercial bioprinted products in clinical use. In order for clinical translation to occur, more process-related knowledge is needed to standardize the bioprinting process so that it is reproducible, customized and safe. In contrast to conventional manufacturing techniques, bioprinted constructs are dependent on both structural and process parameters as well as material properties. Additionally, bioprinting grafts contain living cells which can secrete matrix proteins and remodel the structure, so that the properties are also varying with time. There are no current standards for bioprinting processes or bioprinted materials, the so called 'bioinks'. Currently additive manufacturing terminology is being standardized (ISO/DIS 17296-1), yet such process standards for bioprinted polymers and hydrogels have not yet been introduced. Best practices and production guidelines for bioprinting technologies are therefore urgently needed (Chhaya et al. 2015). The guidelines include careful rheological characterization of the bioinks, mechanical testing of printed grafts and viability assays.

Bioink development is often considered to be the most challenging part of three-dimensional (3D) bioprinting due to the need to simultaneously optimize for high resolution printing, mechanical properties and biocompatibility (Malda et al. 2013). Several articles have related the decrease in cell viability after printing to polymer content (Billiet et al. 2013) or printing pressure (Aguado et al. 2012; Billiet et al. 2014; Müller et al. 2016). However, increasing polymer content and viscosity have been reported to improve printing resolution (Khalil and Sun 2009; Tirella et al. 2009) and mechanical properties (Billiet et al. 2014). The understanding of the rheological properties of bioinks including shear thinning, yield stress, viscosity, shear recovery and crosslinking kinetics are important in evaluating the printing

parameters and material related mechanical properties. Rheological analysis of shear response and shear recovery should be performed to predict the printing pressure and shape retention respectively (Figure 1A). The shear response can be divided into two categories, namely shear thinning or shear thickening, which illustrates the bioink viscosity in shear, thus allowing the printing pressure to be predicted.

Mechanical characterization of the printed structures is important to evaluate how stable the printed structures will be in the intended implantation site. Furthermore, the relevance of a correct match of the deformation behavior of the implant material and of the underlying tissue has recently been shown (Mazza and Ehret 2015). These properties are a function of the material itself, as well as bioprinting process parameters (Figure 1B). Printed tensile specimens have been used to investigate the interaction of lines and layers (Bakarich, Balding, et al. 2014; Bakarich, Gorkin, et al. 2014; Compton and Lewis 2014; Cui et al. 2012; Hong et al. 2015; Kesti et al. 2015; McKee et al. 2011; Mueller, Shea, and Daraio 2015; Wei et al. 2015), however, a systematic investigation of how process parameters influence these properties has not been conducted. Terminology to describe the tensile measurements include two crucial aspects. First, the displacement to calculate strain can be reported in terms of global or local (true) displacement (Figure 1C). The latter is the preferred value and reflects deformation of the gauge length of the specimen, where global displacement is more susceptible to artifacts (e.g. slippage) and/or material deformation inhomogeneities. Secondly, it is important to specify whether the stress is reported as 1st Piola-Kirchhoff stress (PK-stress = force divided by initial cross sectional area) or Cauchy stress (C-stress = force divided by current cross sectional area) (Figure 1D). The second definition of stress becomes relevant when deformations in the gauge become large, leading to a significant difference between initial (reference) and deforming (deformation) cross sectional area; e.g. in the case

of hydrogels (Supplementary Figure 1). C-stress however requires a visual acquisition of the specimen shape during the measurement, something which is not always available in tensile testing setups.

Currently the printing properties of bioinks are mainly characterized by rheology and allow the effects of sterilization, storage or batch production to be quantified. Additional mechanical tensile tests are required to determine how printing process parameters such as line spacing and printing pressure affect structural properties of the printed constructs. Using a physically crosslinkable gellan-alginate bioink called *Vivoflow*, we performed a parametric study to identify and to quantify the parameters with the greatest effect on mechanical properties of bioprinted structures. Furthermore, we demonstrated how these complementary material (rheology) and process related (tensile) measurements can be used to evaluate and compare bioinks. Best practice guidelines are presented so that future bioink developers can evaluate their product according to common standards.

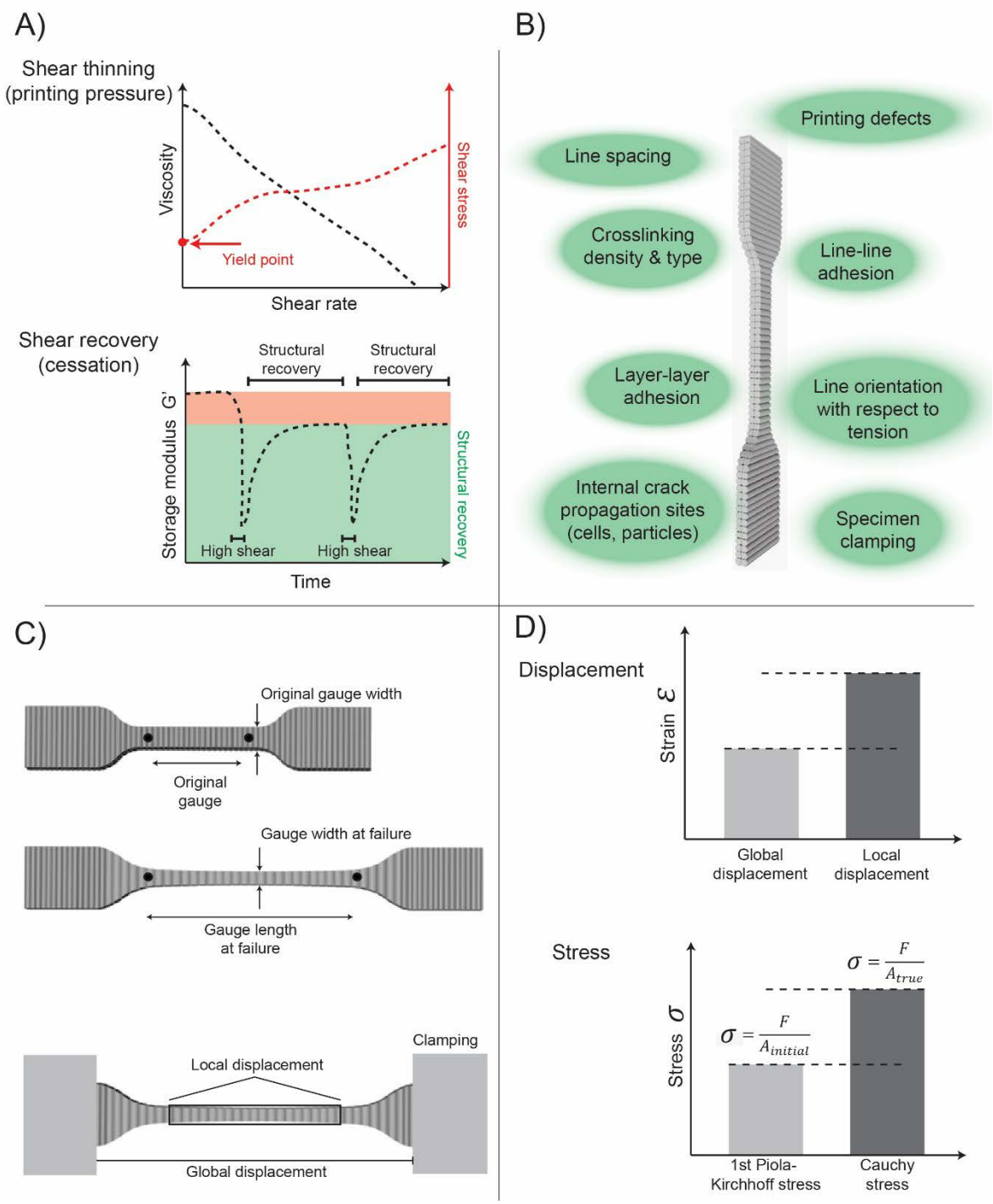

Figure 1. A schematic illustration of the important rheological and mechanical characteristics of bioprinted structures. Rheological measurements of shear rate vs viscosity shows shear thinning which is important for printability and required printing pressure while the measurement of shear recovery (cessation) is important to evaluate shape retention post-printing A). Bioprinting process parameters affecting the mechanical properties of the printed

structures B) and how typical hydrogel dumbbell specimens deform in tension B) are further illustrated. Tensile properties should be calculated based on a strain derived either using global displacement (based on the distance between the grips) or local (true) displacement (measured from the video tracking of the displacement in the gauge length). Furthermore, the stress can be given as 1st Piola-Kirchhoff stress (calculated using the initial cross sectional area) or as Cauchy stress (using true cross sectional area) D). The measurements and their calculation should always be described using these terms so that studies can be compared and reproduced.

Results

A parametric study was performed with the *Vivoflow* bioink to investigate the most important material and bioprinting process parameters to obtain reproducible bioprinting. As a first step, printing process parameters such as pressure, feed rate and printing height were tested to standardize the line thickness to 982 um ± 92 um (Supplementary Figure 2). After determination of the average line thickness, the effective line-line adhesion was investigated by printing a series of bioink sheets with different line spacing (Figure 2). At all line spacings between 400-700 microns, there was a continuous overlap of the printed lines. Based on these observations, the effect of line spacing in this range on tensile properties was investigated by comparing printed and cast (bulk) dumbbell samples of the same bioink. The line orientation was perpendicular to the tensile direction (transverse, 90°) to maximize the influence of line-line adhesion. As seen from the variance in ultimate stress, when a wider line spacing (600-700µm) was used, an increasing number of specimens broke before the sample could be mounted in the testing device. However, for the samples that could be tested, some of them were in fact as stiff as the samples printed with the smaller line spacing (400-500µm). Similar behavior was observed for ultimate strain where nearly 50% strain was achieved with all line

spacing conditions, when the test could be carried out. As illustrated in Figure 2 the most reproducible printing quality was achieved with the line spacing of 500 μm, thus all the following experiments were conducted with the dumbbell specimen printed with this line spacing.

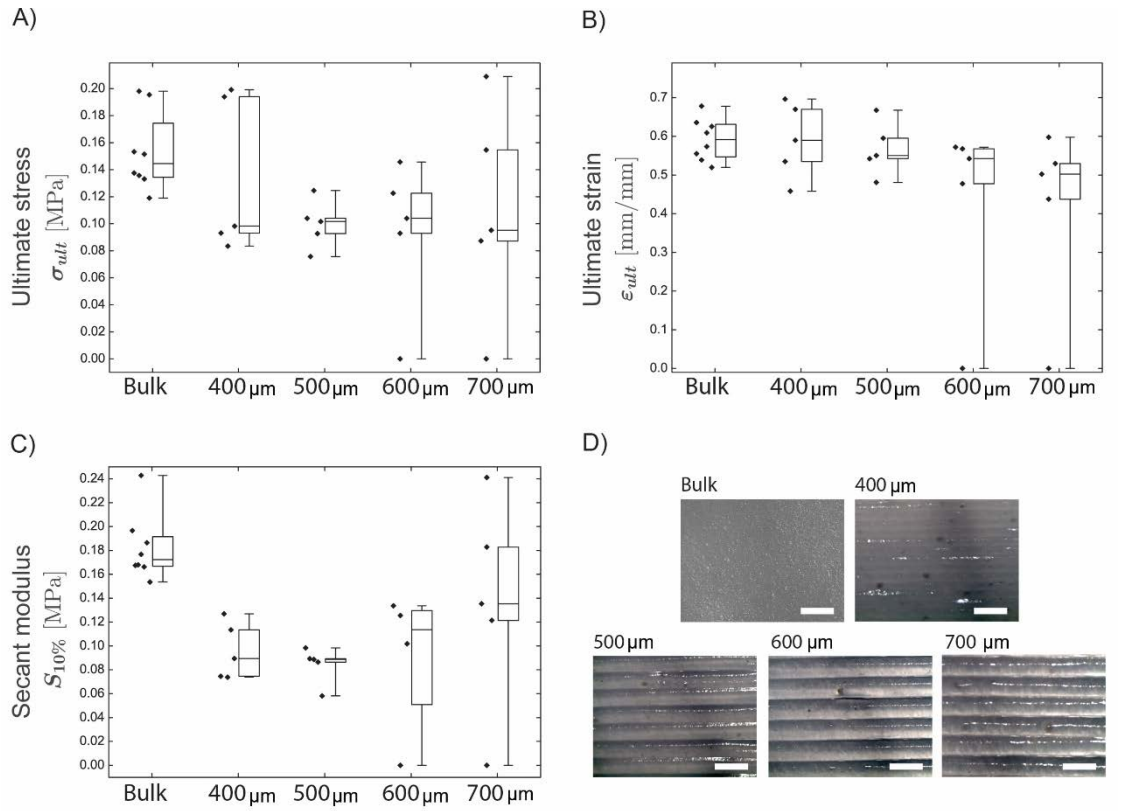

Figure 2. With increasing line spacing, there is an increased probability of defects in line-line adhesion in comparison to cast samples (bulk). A) Ultimate stress (Cauchy), B) ultimate strain (local) and C) secant modulus (<10%) illustrate how probability of structural defects due to the printing process increased with the increasing line spacing. Each point represents a tensile specimen at failure and the values are represented also by boxplots where 50% of the values are in the box, middle line is the mean and tails represent the highest and the lowest values. The microscopy image for each line spacing shows the change in surface topography D).

Bioprinting process allows fabrication of complex shapes which can ultimately be used in regenerative medicine as organ templates and other complex tissue replacement grafts. These complex structures will inevitably be exposed to forces acting in arbitrary directions, thus the printing direction should not in general affect the structural properties. A parametric investigation of printing direction with respect to the direction of tensile load was performed. Dumbbell specimens were printed parallel (0°), transverse (90°) and at 45° to the direction of tensile loading. In Figure 3A no significant change in the ultimate stress ($p>0.1$), ultimate strain ($p>0.1$) or secant modulus ($p>0.1$) was observed when the printing direction was altered, thus illustrating that the printing direction is not a significant factor in withstanding the external forces acting on the printed structures if the line spacing is optimized.

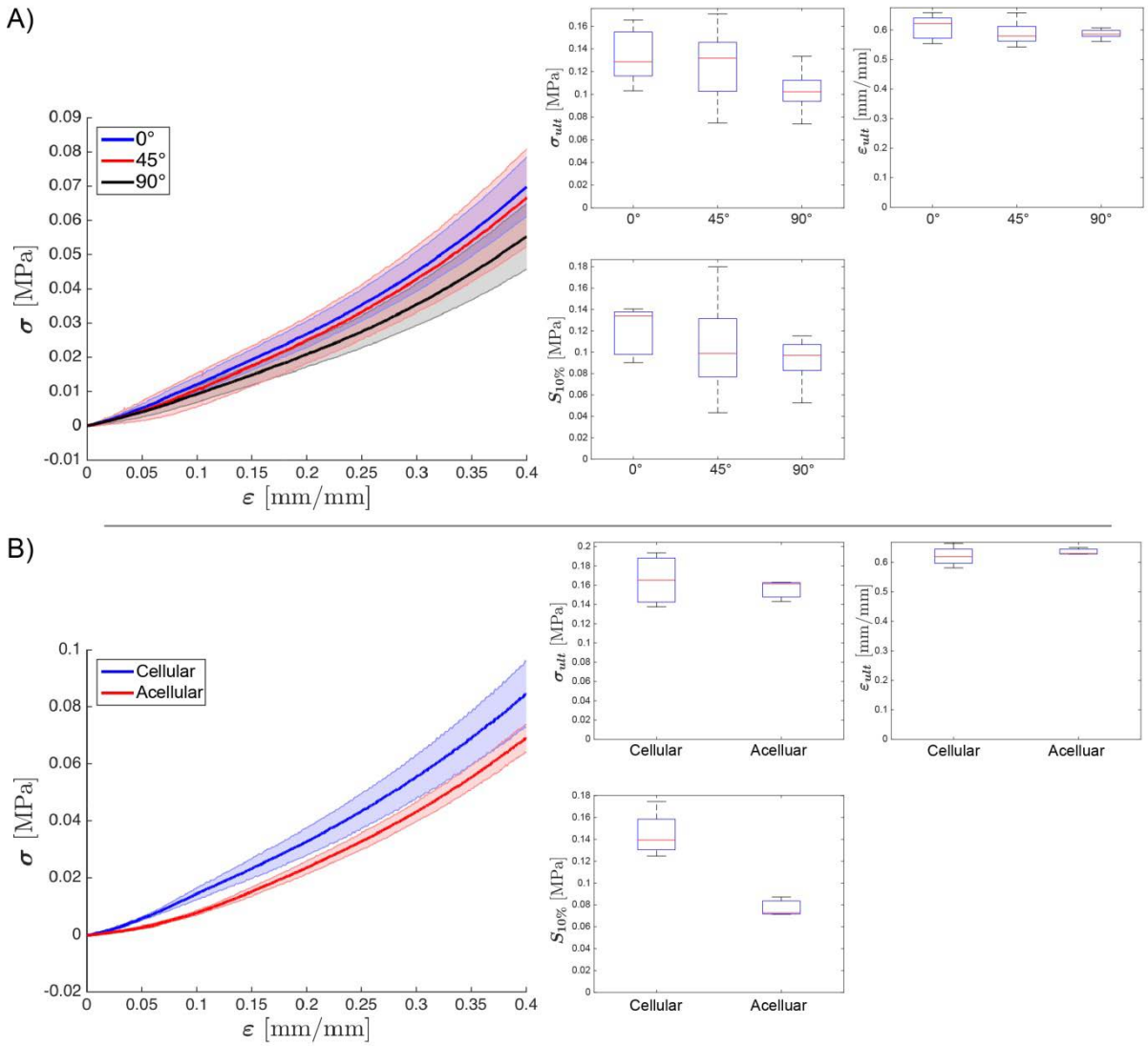

Figure 3. Tensile measurements of specimens with varying printing direction A) and comparison of cellular and acellular specimens B). The dumbbell specimens were printed in longitudinal (0°), transverse (90°) or diagonal (45°) orientations with respect to the tensile direction. No significant differences were observed in ultimate stress (Cauchy), ultimate strain (local) or secant modulus (<10%) as a function of the printing direction. Furthermore, there was no significant differences in ultimate stress and strain when tensile properties of cell laden and acellular specimens were measured ($6x10^6$ cells/ml, ~1% v/v) while a significant difference in secant modulus was observed. The shaded regions of the stress-strain curve represent standard deviation (n=5).

Bioinks are often tested for mechanical properties without cells, although final applications include cells. Figure 3B however confirms that no significant difference in the ultimate stress ($p > 0.1$) and ultimate strain ($p > 0.1$) were found through addition of $6x10^6$ cells/ml (equivalent to ~1% (v/v) volume fraction of cells). However, the secant modulus was significantly higher ($p < 0.005$) with cells, which might reflect the slight cell cation interactions which are not significant when the structure is subjected to increased mechanical loading.

Direct comparison of bioink properties is important in order to be able to select specific inks for specific applications. A standardized testing protocol consisting of rheological and mechanical assessments was used to compare three commercially available bioinks to Vivoflow, which was physically crosslinked with cations for one and 24 hours (Kesti et al. 2015). The commercial bioinks are referred to based on their main composition as **Gel-MA** (10% gelatin methacrylate photo-crosslinked with 0.05% Ircacure I2959, BioGel from BioBots) (Billiet et al. 2014; Hoch et al. 2012; Schuurman et al. 2013), **PEG-DA** (polyethyleneglycol-diacrylate photo-crosslinked with photoinitiator, BioInk from regenHu AG, (Rimann et al. 2015) and **NC-Alg** (1.36% nanocellulose and 0.5% alginate crosslinked with cationic solution, Cellink from Cellink) (Markstedt et al. 2015). The rheological tests included shear behavior with yield point measurements (Figure 4A) and shear recovery analysis by two shear cycles (Figure 4B). In all bioink compositions a clear shear thinning behavior was observed whereas yield point was only observed in Vivoflow (31Pa ± 2.4Pa), Gel-MA (65Pa ±14 Pa) and NC-Alg (11Pa ± 0.7Pa). PEG-DA bioink did not have a yield point and is the only ink not designed to have shape forming and viscous fluid like properties in printing. The shear recovery behavior, i.e. bioink's ability to recover structural stability

(stop flow and to withstand consecutive line printing), was high in all the bioink compositions (> 79%) whereas the storage modulus was too low to withstand consecutive layers in PEG-DA. Briefly, Vivoflow and PEG-DA recovered fully (> 99%) after the shear whereas storage modulus recovery up to 79.3% in NC-Alg and 84.3% in Gel-MA was observed. Furthermore, the shape retention capability and stiffness of the Vivoflow, Gel-MA and NC-Alg were sufficient for consecutive layer printing without intermediate crosslinking whereas the PEG-DA required crosslinking before consecutive layers could be built.

Mechanical properties of the printed structures were characterized in order to evaluate structural integrity. Figure 4F illustrates the secant modulus of all the bioinks (measured at 10% strain) which was confirmed to be within the elastic deformation zone. Vivoflow 1hr had significantly higher modulus compared to all the other commercial bioinks ($p<0.01$) and furthermore Vivoflow 24h had significantly higher modulus ($p< 0.05$) compared to Vivoflow 1h. The secant modulus of the other commercial bioinks were not significantly different from each other ($p>0.05$). Similarly, Vivoflow 24h had the highest ultimate stress (183kPa ± 36kPa, $p<0.001$) whereas the other conditions were not statistically significantly different (Vivoflow 1h 39kPa ± 8.9kPa, Gel-MA 22kPa ± 20kPa, PEG-DA 18kPa ± 7kPa and NC-Alg 1.4kPa ± 0.2kPa). Ultimate strain value of Vivoflow 24h was similar to the covalently crosslinked bioinks (PEG-DA, Gel-MA) ($p>0.05$) whereas the NC-Alg had significantly lower ultimate strain value compared to Vivoflow 24h ($p<0.005$), Gel-MA ($p<0.05$) and PEG-DA ($p<0.05$). All the secant modulus, ultimate stress and ultimate strain values for each bioink can be found in Supplementary Table 1.

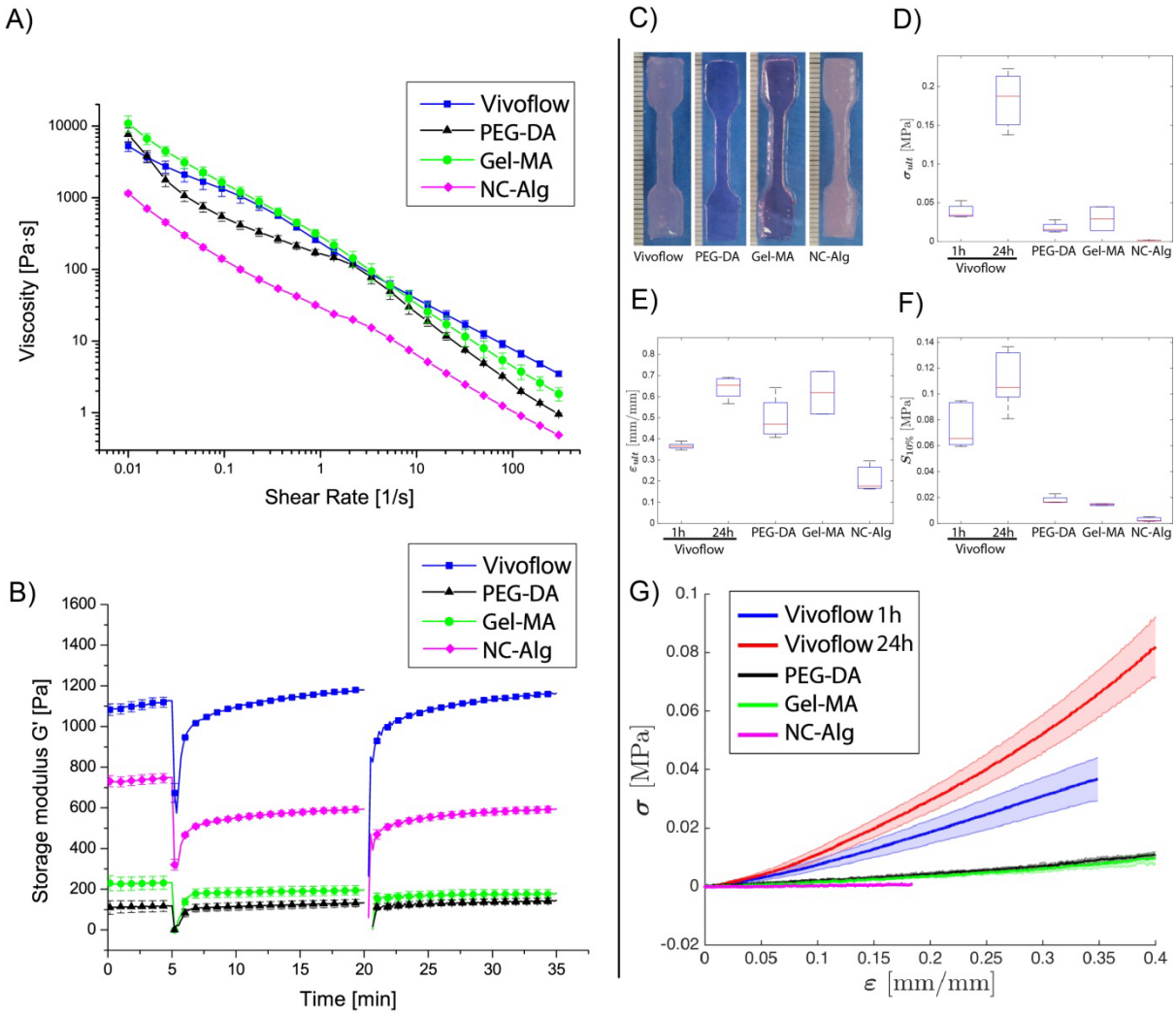

Figure 4. Comparison of rheological properties (A-B) and mechanical testing (C-G) of three commercial bioinks and Vivoflow. Shear thinning behavior was observed in all the bioink compositions (PEG-DA, Gel-MA, NC-Alg) A) and shear recovery curves for all the bioinks suggested high levels of recovery (> 79%) B). Mechanical properties of tensile specimens C) with ultimate stress (Cauchy) D), ultimate strain (local) E), secant modulus (< 10%) F), and average stress-strain curves for each bioink G) are shown. Error bars (D-F) and shaded regions (G) represent standard deviation. Each condition was tested with minimum of n=3 in rheology and n=4 in tensile testing.

The Vivoflow bioink can be tuned to match the desired tissue properties, thus the compatibility with several different cell types can be enhanced. Tensile tests were performed

after crosslinking with 20mM $SrCl_2$ for 0.5, 1, 3, 6, 12, and 24 hours to investigate the crosslinking kinetics and effect on mechanical properties. The ultimate stress increased from 24kPa ± 3.2kPa up to 140kPa ± 29kPa with 20mM $SrCl_2$ during 24 hours of crosslinking whereas ultimate strain increased from 30% ± 1.2% to 58% ± 3.7% in the same period. Furthermore, the tensile properties were evaluated after crosslinking with 20mM, 50mM and 100mM strontium or calcium chloride. When the cation concentration was increased from 20mM to 100mM, the ultimate strain was not significantly different illustrating preservation of the construct elasticity whereas the ultimate stress increased from 121kPa ± 39kPa to 197kPa ± 51kPa for $SrCl_2$ and from 106kPa ± 13kPa to 228kPa ± 19 kPa for $CaCl_2$. Similarly secant modulus increased significantly when cation concentration was increased. Similar results for pure gellan gum gels (Grasdalen and Smidsrød 1987) and pure alginate gels (Mørch et al. 2006) have been previously reported.

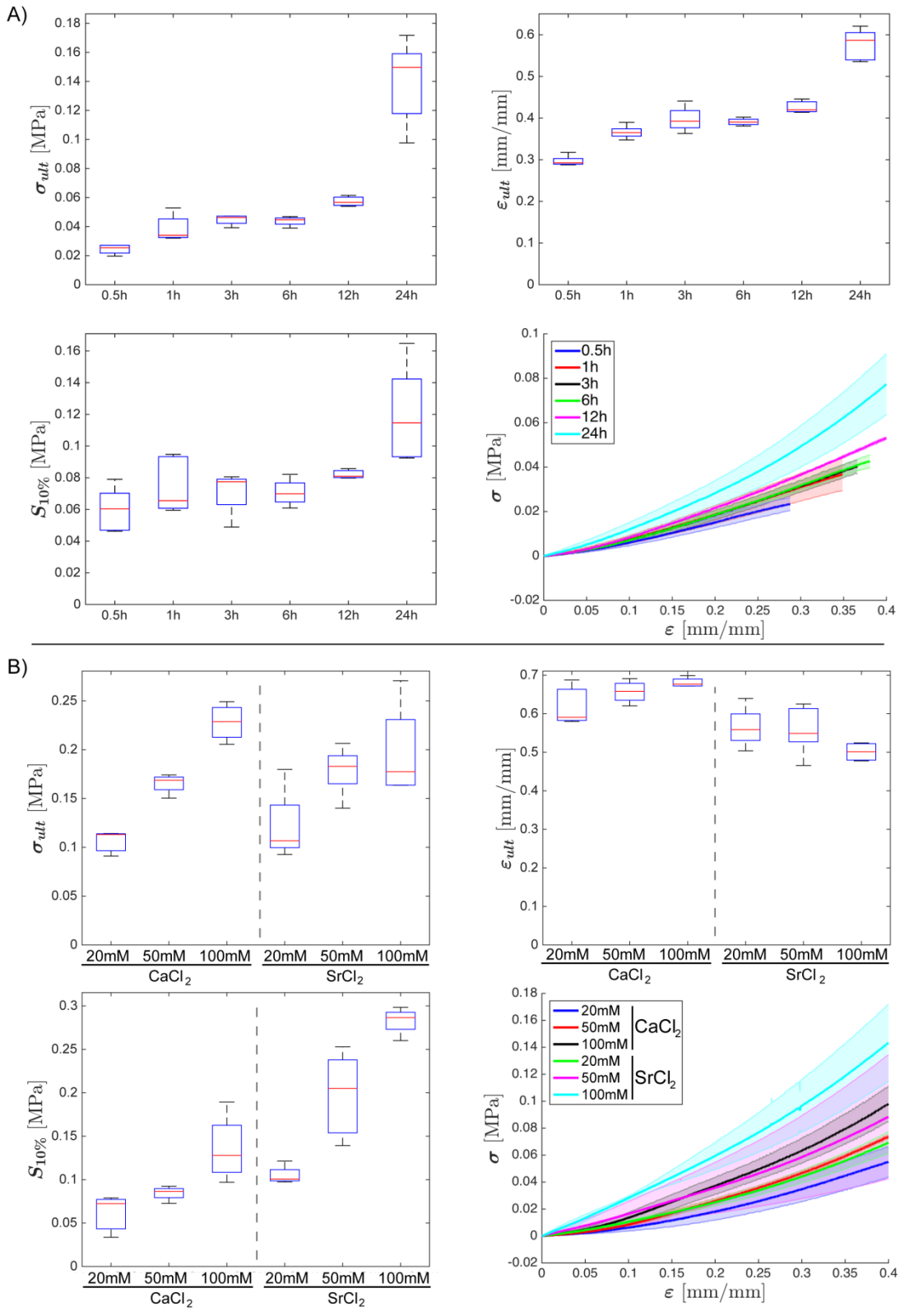

Figure 5. Mechanical properties of the Vivoflow printed grafts are tunable by crosslinking time A) and concentration and cation source B). The mechanical properties from lowest to highest were achieved between the crosslinking conditions 20mM $SrCl_2$, 0.5h and 100mM

$SrCl_2$, 24h. The mechanical properties can be tuned after the bioprinting process which allows more cell specific approaches. The shaded regions in the stress-strain curve represent standard deviation. Each condition was tested with five samples (n=5). Ultimate stress (Cauchy), ultimate strain (local) and secant modulus (<10%) are represented.

Vivoflow Bioink was designed for cartilage bioprinting (Kesti et al. 2015) and primary bovine chondrocytes were mixed into the ink prior to printing. The cell laden bioprinted structures were monitored over 21 days for the changes in cell viability and amount of DNA. High cell viability (>93%) was observed over the whole 14 day period in vitro culture which is the minimum recommended time to observe viability in bioinks. Furthermore, double stranded DNA was quantified over 21 days to assess cell proliferation in the bioink. The amount of DNA doubled over 21 day culture in vitro suggesting that the bioink and bioprinting process were cell compatible.

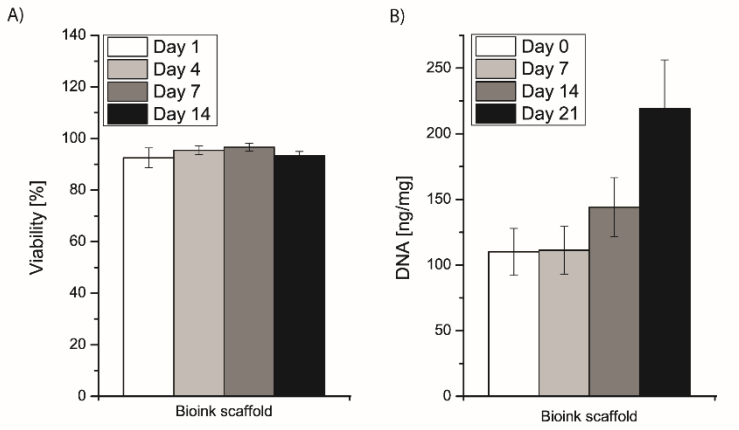

Figure 6. Biocompatibility assays performed for Vivoflow printed scaffolds. Viability of the embedded cells A) and DNA quantification as a measure of proliferation B). The error bars represent the standard deviation and each condition was tested with n=8 and n=6, respectively.

Discussion

Bioprinting allows precise deposition of cell-laden inks in a confined 3D space. The high precision manufacturing process is prone to bioink- and process-related effects which can lead to variable mechanical properties and poor reproducibility. This paper evaluates and quantifies the mechanical properties of bioprinted structures compared to non-printed cast structures to determine the optimal printing process parameters. A systematic study was performed to investigate and to quantify the most important bioprinting process parameters in order to provide accurate process knowledge and best practices for reproducible bioprinting. Furthermore, this study provides guidelines for standardized bioink testing so that future bioinks can be compared to current ones (Table 1).

The results suggest that the most important parameters for the optimized and reproducible bioprinting processes with pneumatic printing systems are constant line thickness and line spacing. In fact, during pneumatically driven extrusion, slight changes in the bioink viscosity introduce flow inhomogeneities, which cause inconsistent line dimensions and line overlap and therefore decreased reproducibility. These local viscosity changes can be present due to bioink additives such as polymers, cells, growth factors, particles and/or entrapped air (Supplementary Figure 3). Polymer chain entanglements and molecular interactions will introduce local viscosity changes that are more frequently present in high polymer concentrations and in more complex compositions. For this reason, a line overlap percent should be introduced to the bioinks to guarantee high reproducibility of the mechanical properties. This line overlap percentage is bioink dependent: for Vivoflow ink, a line overlap of >48% produced constant and reproducible structural properties. Furthermore, the ultimate stress and ultimate strain of the cast and the printed specimens with this line overlap percentage (500µm line spacing) were not statistically different. These results suggest that

with optimized bioprinting process and line overlap, it is possible to produce reproducible structures with comparable mechanical properties to cast structures. To minimize the line overlap percentage the pneumatically driven extrusion systems could be replaced with the piston driven (positive displacement) systems to gain a full control over the dispensing volume over time despite the presence of minor irregularities and local viscosity changes.

Production of complex tissue constructs and organ templates in the bioprinting process are rarely assessed for their mechanical integrity. Complex anatomic structures cannot yet be printed with controlled mechanical anisotropy, thus the printing direction should not introduce differences in mechanical properties. A recent study by Compton et al. (Compton and Lewis 2014) described how internal fiber-reinforcement increased the mechanical properties in epoxy based materials and significant differences were reported between the transverse and longitudinal samples in tension. These differences were explained by the high aspect ratio fibers capability to bind to the polymer matrix with high pullout stress and up to nine times Young's modulus was achieved compared to the casted polymer resin without fibers. Müller et al. investigated inkjet printing process parameters with photo-curable acrylic based rigid (VeroWhitePlus) and rubber-like (TangoBlackPlus) materials in alternating layers. The transverse (90°) and longitudinal (0°) printing directions were found significantly different in ultimate stress and strain values with no differences in the Young's modulus (Mueller et al. 2015). Figure 3 illustrates the hydrogel based bioink comparison in different printing directions with an optimized printing process. These experiments did not show significant differences between longitudinal, diagonal and transverse testing directions for secant modulus, ultimate stress or ultimate strain, thus illustrating that the printing direction was not a significant factor. However, if the line spacing is increased beyond the line overlap

percentage, differences between the printing directions could become significant due an increased probability of discontinuous line adhesion.

Translation of bioprinting technologies to industrial and clinical products has been limited by several drawbacks such as poor reproducibility of the printing process and scarcity of commercial bioinks. Furthermore, the lack of standardization limits the application driven product design needed for clinical products. A standardized test protocol consisting of rheological and mechanical characterization was introduced for direct comparison of bioinks. All tested bioinks had shear thinning properties, which is essential for cell survival during the extrusion process, and high shear recovery behavior (>79%). This illustrates the material's capacity to preserve the extrusion resolution and support layers before further crosslinking. The limited shear recovery of the Gel-MA and NC-Alg bioinks can be explained by the structural changes in the polymer components during the high shear which can result in weaker structures post-printing; however, both bioink had sufficient recovery for consecutive layer printing without intermediate crosslinking similar to Vivoflow, whereas the PEG-DA bioink required layer-by-layer crosslinking. Mechanical comparison of current commercial bioinks revealed similarities in ultimate stress and secant modulus, while the covalently crosslinked bioinks outperformed the physically crosslinked NC-Alg in ultimate strain. Physically crosslinked Vivoflow had the highest secant modulus of all the bioinks despite the crosslinking time and the overall highest ultimate stress was achieved with Vivoflow 24 hr. Furhermore, the ultimate strain of Vivoflow 24h was similar to the covalently crosslinked bioinks illustrating the strong physical crosslinking.

The Vivoflow bioink was further characterized in detail for its crosslinking-dependent mechanical (Figure 5) as well as biological properties (Figure 6). Mechanical properties were

found to be highly dependent on the crosslinking conditions such as crosslinking time, concentration and cation source. Vivoflow crosslinking was found to be time dependent, driven by the osmosis and the diffusion properties of the increasingly crosslinked matrix. The highest recorded secant modulus (283kPa ± 16kPa) and highest ultimate stress (197kPa ± 51kPa) were achieved with the 100mM $SrCl_2$ crosslinking in 16 hours. Intermediate crosslinking properties were recorded with one hour crosslinking which was also tested for the biocompatibility with embedded chondrocytes ($6x10^6$ cells/ml) for tissue engineering applications. The bioink volume fraction of the cells was approximately 1% and had no significant differences in ultimate stress or ultimate strain values although a significant difference in secant modulus was observed in cellular specimen, suggesting cells ability to affect in cation-polymer interactions, thus stiffening the bioink. Neither the printing process nor the crosslinking compromised cell viability over the 14 days observation period; in fact, during 21 days the amount of DNA doubled in the cellular constructs illustrating good biocompatibility.

Here we systematically investigated the bioprinting process parameters to determine the optimal conditions for biocompatible printing. The influence of parameters on structural integrity were systematically evaluated and quantified for the best practices (Table 1). This process-related knowledge and its influence on mechanical properties are essential for modelling, design and production of fabricated biological structures. Since most of the effects are related to fundamental process parameters, the results are applicable to other bioprinting setups which use extrusion (pneumatic or displacement), microvalve mediated and laser-based bioprinters. This paper aims to establish common standards for bioprinting process and protocols for bioink characterization which can benefit the whole community.

Table 1: Best Practices and Guidelines for Bioprinting

Guidelines for optimized bioprinting

Method	Action	Importance (1-5)
Rheology	Characterize ink by measuring shear thinning and shear recovery	5
	Evaluate effect of sterilization and storage on rheology	5
Printing process parameters	Optimize the printing line dimensions by feedrate, pressure, nozzle dimension and nozzle height	5
	Optically determine the line spacing until overlap occurs	3
	Investigate the line overlap percentage for reproducible mechanical properties (where casted and printed specimens have analogous properties)	5
Tensile tests	Perform tensile testing according to standardized protocol (refer. ISO & ASTM standards)	5
	Report secant modulus at 10% strain (if linear approximation is valid)	3
	Report which calculation, initial strain or true strain and C-stress or PK stress, is used	5
	Evaluate effect of sterilization and storage on mechanical properties	3
Biocompatibility	Viability tests are carried for a minimum of 2 weeks and augmented with proliferation and protein synthesis assays	5
	Assure that the printing process does not adversely affect cellular function or phenotype	4

Materials and Methods

Gellan (Kelcogel) was purchased from the CP Kelco in both high and low acetylated forms. High G content alginate was purchased from Kimica, Chile ltd. D-glucose was purchased from Sigma-Aldrich (Buchs, Switzerland). Dulbecco's modified Eagle's media (DMEM), phosphate buffered saline (PBS), fetal bovine serum (FBS), penicillin-streptomycin (PS), and

trypsin were all purchased from Life Technologies (Zug, Switzerland). All concentrations are given in percentages weight/volume (% w/v) unless otherwise indicated.

Bioink preparation: Gellan was added to D-glucose (300mM) containing ultra-pure water at 90°C to achieve a 3.5% solution and alginate was added to the mixture to achieve 2.5% solution. The boiling flask was kept at 90°C with agitation until the solution was homogeneous, typically for one hour. The homogeneous solution was cooled down to ~30°C prior the cell mixing. Briefly, the bovine chondrocytes (6 $x10^6$ cells/ml) passage two were mixed in the culture medium consisting of DMEM, 10% FBS, 1 % PS, 50µg/ml ascorbic acid and 10ng/ml of transforming growth factor beta three (TGF-β3) added to the bioink in 1:10 volume ratio whereas acellular bioink was mixed with culture medium without cells and TGF-β3 to pre-crosslink the bioink. Mixing was performed until the solution reached room temperature and the printing syringes were loaded. For the best printing outcome with acellular bioink, the syringes were centrifuged at 5000rpm for 8min for degasing.

Commercial bioinks: All commercial bioinks were purchased from the original vendors Cellink (Advanced Polymer Technology, Sweden), BioInk (RegenHU, Switzerland) and BioGel (BioBots, US). The inks were prepared according to manufacturer's protocols and recommendations except in BioGel where a common photoinitiator, Ircacure® 2959 in cytocompatible 0.05% concentration (Bryant, Nuttelman, and Anseth 2000; Williams et al. 2005), was used instead of the one provided by the vendor. Commercial inks were crosslinked with two different methods: photo-crosslinked (BioInk and BioGel) and physically crosslinking via cations (Vivoflow, Cellink). Photo-crosslinking was performed for 1min following each layer and finally for 5min to complete the crosslinking whereas the cation initiated bioinks were crosslinked post printing for 10min with Cellink kit crosslinking solution and 1h or 24h for Vivoflow (20mM $SrCl_2$).

Printing syringes of the bioinks were mounted onto the extrusion printer Biofactory® (RegenHU, Switzerland) and the parameters were set for 410 micron straight nozzle diameter. The BioInk (P:50-125 kPa, valve opening time 200µs) and the Cellink (P:35 kPa, valve opening time 1200µs) were printed according to manufacturer's recommendations using pneumatic microvalves whereas BioGel was printed with a direct extrusion system as suggested by the manufacturer similar to Vivoflow. Immediately following the printing, the tension dumbbells were transferred into sterile petri dishes containing either the crosslinking medium (Cellink and Vivoflow) or culture medium (BioInk, BioGel). Following the physical crosslinking all the samples were kept in culture medium for 48 hours to allow uniform swelling before the mechanical testing. In the results, the commercial inks are referred to by their composition: Bioink = **PEG-DA**, BioGel = **Gel-MA**, Cellink = **NC-Alg**.

Rheology: An Anton Paar MCR 301 (Anton Paar, Zofingen, Switzerland) rheometer equipped with a Peltier element for temperature control and a thermostatic hood was used to measure the bioinks to determine shear and recovery responses by simulating the bioprinting. Shear thinning was analyzed in rotation with a plate-cone geometry (50 mm diameter) by measuring viscosity η at a frequency of 1 rad s^{-1} with logarithmic increase of shear rate. Yield points were calculated using the Herschel/Bulkley equation

$$\tau = \tau_{HB} + c \cdot \dot{\gamma}^{p}$$

where τ is shear rate, τ_{HB} is the Herschel/Bulkley yield point, c flow coefficient, $\dot{\gamma}^{p}$ shear stress with exponent p, where p is the Herschel/Bulkley index ($p < 1$ for shear thinning and $p > 1$ for shear thickening). Cessation of flow was measured for each bioink in oscillation with a frequency of 1 rad/s and 1% strain for 15min sequence until a one second lasting high shear (100^{-s}) sequence was performed followed by oscillation and second high shear sequence. All

the rheology measurements were performed at 25°C corresponding to the printing at room temperature and all the measurements were measured in triplicates.

Mechanical testing: Mechanical testing was performed by considering the guidelines and standards for elastomers and plastics in tensile measurements (ASTM D412-06a, ASTM D638-14, ISO 37, ISO 527-1,2) as well as standards for biomedical and regenerative medicine (ASTM F2064-14, ASTM F2900-11, ASTM F2150-13). Bioinks were printed in sheet conformation (4cm length, 1cm width and 1.5mm height) to prevent printing related stress localization and inaccurate sample sizes. The sheets were kept in culture medium for 24hours for uniform swelling and the dumbbell specimens were stamped according to ISO 527-2-5B standard. The cast bioink sheets (bulk) were similarly stamped. Each specimen was imaged with a stereomicroscope (Wild M650, Leica) to calculate the initial gauge dimensions where the average height and width were averaged from three sample positions (Supplementary Figure 4). Tension testing was performed with a custom-made testing device with uniaxial hydraulic actuators equipped with a 100N load cells. Custom-made titanium clamps equipped with sandpaper for specimen fixation where bioink dumbbells were between 1.5-2mm in thickness comprising of 2 printed layers. The tensile specimens were clamped to the retracting probes without preloading and the stress-strain curves were recorded after 0.005N - 0.01N tensile force was applied. Samples were subjected to a controlled tensile displacement of 0.1 mm s^{-1} until failure in a saline bath (NaCl, 154mmol/L) at room temperature. Local (true) strains were determined from images of the deforming specimens (time lapse) via point tracking with a custom-written code or similarly using an ImageJ plugin trackmate. Both 1st Piola-Kirchhoff (σ_{PK1}) and Cauchy (σ_C) stresses were computed for each specimen according to the following relations: $\sigma_{PK1} = F_c/(w_0 t_0)$, and $\sigma_C = F_c/(w_c t_c)$, F being the measured force throughout the tensile test, w the specimen width, and t its thickness where the

subscripts 0 and c refer to the initial (reference) and the current (deformed) configurations, respectively. Each specimen dimensions (width and thickness) were measured using a stereomicroscope (Wild M650, Leica) initially (reference) and a poisson ratio was analyzed from the local deformation tracking to simulate the thickness changes during the deformation (deformed). Secant modulus was calculated within the linear region of the stress-strain curve by dividing the corresponding stress value by the 10% strain. A linear region was observed until 10% strain for all the tension samples where the secant modulus highly correlates with the Young's modulus. Ultimate stress was always calculated using Cauchy stress equation and ultimate strain was always determined from the local deformation. These ultimate values were obtained as the highest values of the stress-strain curves which were recorded until 0.5% decrease in the stress was detected to neglect any disruption related forces.

Acknowledgements

The work was funded by the Swiss National Science Foundation (grant number CR32I3_146338 / 1) and FIFA/F-MARC. Authors would like to thank Prof. André Studart, Complex Materials, ETH Zurich for use of equipment.

References

Aguado, B., Mulyasasmita, W., Su, J., Lampe, K., and Heilshorn, S., (2012). Improving Viability of Stem Cells During Syringe Needle Flow Through the Design of Hydrogel Cell Carriers. Tissue Eng. Part A. 18, 806–15.

Bakarich, S., Balding, P., Gorkin, R., Spinks, G. M., and In het Panhuis, M. (2014). Printed Ionic-Covalent Entanglement Hydrogels from Carrageenan and an Epoxy Amine. RSC Advances 4, 38088–38092.

Bakarich, S., Gorkin, R., In Het Panhuis, M., and Spinks, G. M. (2014). Three-Dimensional Printing Fiber Reinforced Hydrogel Composites. ACS applied materials & interfaces 6(18),15998–16006.

Billiet, T., Van Gasse, B., Gevaert, E., Cornelissen, M., Martins, C. J., and Dubruel, P. (2013). Quantitative Contrasts in the Photopolymerization of Acrylamide and Methacrylamide-Functionalized Gelatin Hydrogel Building Blocks. Macromolecular bioscience, 13(11), 1531–1545.

Billiet, T., Gevaert, E., De Schryver, T., Cornelissen, M., and Dubruel, P. (2014). The 3D Printing of Gelatin Methacrylamide Cell-Laden Tissue-Engineered Constructs with High Cell Viability. Biomaterials 35(1), 49–62.

Bryant, J. S., Nuttelman, R. C., and Anseth, S. K. (2000). Cytocompatibility of UV and Visible Light Photoinitiating Systems on Cultured NIH/3T3 Fibroblasts in Vitro. J. Biomat. Sci. Polymer Edn, 11(5), 439–457.

Chhaya, P. M., Poh, SP. P., Balmayor, R. E., van Griensven, M., Schantz, J-T., Hutmacher, W. D. (2015) Additive Manufacturing in Biomedical Sciences and the Need for Definitions and Norms. Expert Rev. Med. Devices, 12(5), 537-543

Compton, G. B., and Lewis, A. J. (2014). 3D-Printing of Lightweight Cellular Composites. Adv. Mat. 26, 5930–5935.

Cui, J., Lackey, M., Madkour, E. A., Saffer, M. E., Griffin, M. D., Bhatia, R. S., Crosby, J. A., and Tew, N. G. (2012). Synthetically Simple, Highly Resilient Hydrogels. Biomacromol. 13(3), 584–588.

Grasdalen, H., and Smidsrød, O. (1987). Gelation of Gellan Gum. Carbohydrate Polymers 7(5), 371–393.

Hoch, E., Schuh, C., Hirth, T., Tovar, M. E. G., and Borchers, K. (2012). Stiff Gelatin Hydrogels Can Be Photo-Chemically Synthesized from Low Viscous Gelatin Solutions Using Molecularly Functionalized Gelatin with a High Degree of Methacrylation. J. mat. sci. Materials in medicine 23(11), 2607–2617.

Hong, S., Sycks, D., Chan, H., Lin, S., Lopez, P. G., Guilak, F., Leong, W. K., and Zhao, X. (2015). 3D Printing of Highly Stretchable and Tough Hydrogels into Complex, Cellularized Structures. Adv. Mat. 27, 4035–4040.

Kesti, M., Eberhardt, C., Pagliccia, G., Kenkel, D., Grande, D., Boss, A., and Zenobi-Wong, M. (2015). Bioprinting Complex Cartilaginous Structures with Clinically Compliant Biomaterials. Adv. Func. Mat. 25(48), 7406-7417.

Khalil, S., and Sun, W. (2009). Bioprinting Endothelial Cells with Alginate for 3D Tissue Constructs. J. Biomec. Eng. 131(11).

Malda, J., Visser, J., Melchels, P. F., Jüngst, T., Hennink, E. W., Dhert, J. W., Groll, J., Hutmacher, W. D. (2013). 25th Anniversary Article: Engineering Hydrogels for Biofabrication. Adv. Mat. 25, 5011–5028.

Markstedt, K., Mantas, A., Tournier, I., Martinez Avila, H., Hägg, D., and Gatenholm, P. (2015). 3D Bioprinting Human Chondrocytes with Nanocellulose–Alginate Bioink for Cartilage Tissue Engineering Applications. Biomacromol. 16(5), 1489–1496.

Mazza, E., and Ehret, E. A. (2015). Mechanical Biocompatibility of Highly Deformable Biomedical Materials. J. Mech. Behav.Biomed. Mat. 48, 100–124.

McKee, T. C., Last, A. J., Russell, P., and Murphy, J. C. (2011). Indentation versus Tensile Measurements of Young's Modulus for Soft Biological Tissues. Tissue Eng. Part B. 17(3), 155–164.

Mørch, A. Y., Donati, I., Strand, L. B., and Skjak-Braek, G. (2006). Effect of Ca2+, Ba2+, and Sr2+ on Alginate Microbeads. Biomacromol. 7, 1471–1480.

Mueller, J., K. Shea, and C. Daraio. 2015. "Mechanical Properties of Parts Fabricated with Inkjet 3D Printing through Efficient Experimental Design." Materials and design 86:902–12. Retrieved (http://dx.doi.org/10.1016/j.matdes.2015.07.129).

Müller, M., Ozturk, E., Arlov, O., Gatenholm, P., and Zenobi-Wong, M. (2016). Alginate Sulfate-Nanocellulose Bioinks for Cartilage Bioprinting Applications. Annals of biomedical engineering.

Rimann, M., Bono, E., Annaheim, H., Bleisch, M., and Graf-Hausner, U. (2015). Standardized 3D Bioprinting of Soft Tissue Models with Human Primary Cells. J. Lab. Autom. 1-14.

Schuurman, W., Levett, P., Pot, W. M., Van Weeren, R. P., Dhert, A. J. W., Hutmacher, W. D., Melchels, P. F., Klein, J. T., and Malda, J. (2013). Gelatin-Methacrylamide Hydrogels as Potential Biomaterials for Fabrication of Tissue-Engineered Cartilage Constructs. Macromol. Biosci. 13, 551–561.

Tirella, A. O., Vozzi, G., and Ahluwalia, A. (2009). A Phase Diagram for Microfabrication of Geometrically Controlled Hydrogel Scaffolds. Biofabrication 1(4), 1-12.

Wei, J., Wang, J., Su, S., Wang, S., Qiu, J., Zhang, Z., Christopher, G., Ning, F., and Cong, W. (2015). 3D Printing of an Extremely Tough Hydrogel. Royal society of Chem. Adv. 5(99), 81324–81329.

Williams, G. C., Malik, N. A., Kim, K. T., Manson, N. P., and Elisseeff, H. J. (2005). Variable Cytocompatibility of Six Cell Lines with Photoinitiators Used for Polymerizing Hydrogels and Cell Encapsulation. Biomat. 26(11), 1211–1218.

High resolution Figures and captions

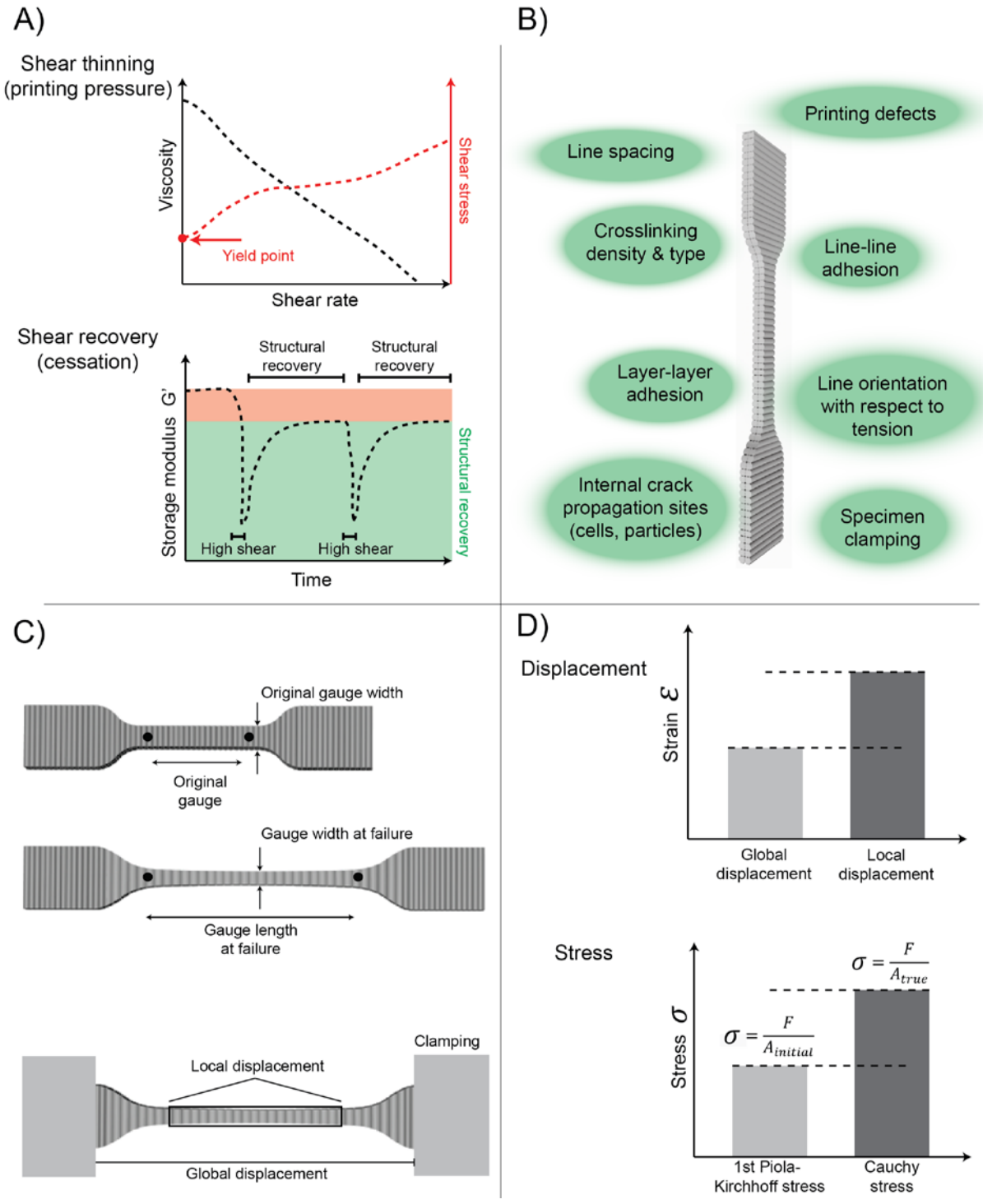

Figure 1. A schematic illustration of the important rheological and mechanical characteristics of bioprinted structures. Rheological measurements of shear rate vs viscosity shows shear thinning which is important for printability and required printing pressure while the measurement of shear

recovery (cessation) is important to evaluate shape retention post-printing A). Bioprinting process parameters affecting the mechanical properties of the printed structures B) and how typical hydrogel dumbbell specimens deform in tension B) are further illustrated. Tensile properties should be calculated based on a strain derived either using global displacement (based on the distance between the grips) or local (true) displacement (measured from the video tracking of the displacement in the gauge length). Furthermore, the stress can be given as 1st Piola-Kirchhoff stress (calculated using the initial cross sectional area) or as Cauchy stress (using true cross sectional area) D). The measurements and their calculation should always be described using these terms so that studies can be compared and reproduced.

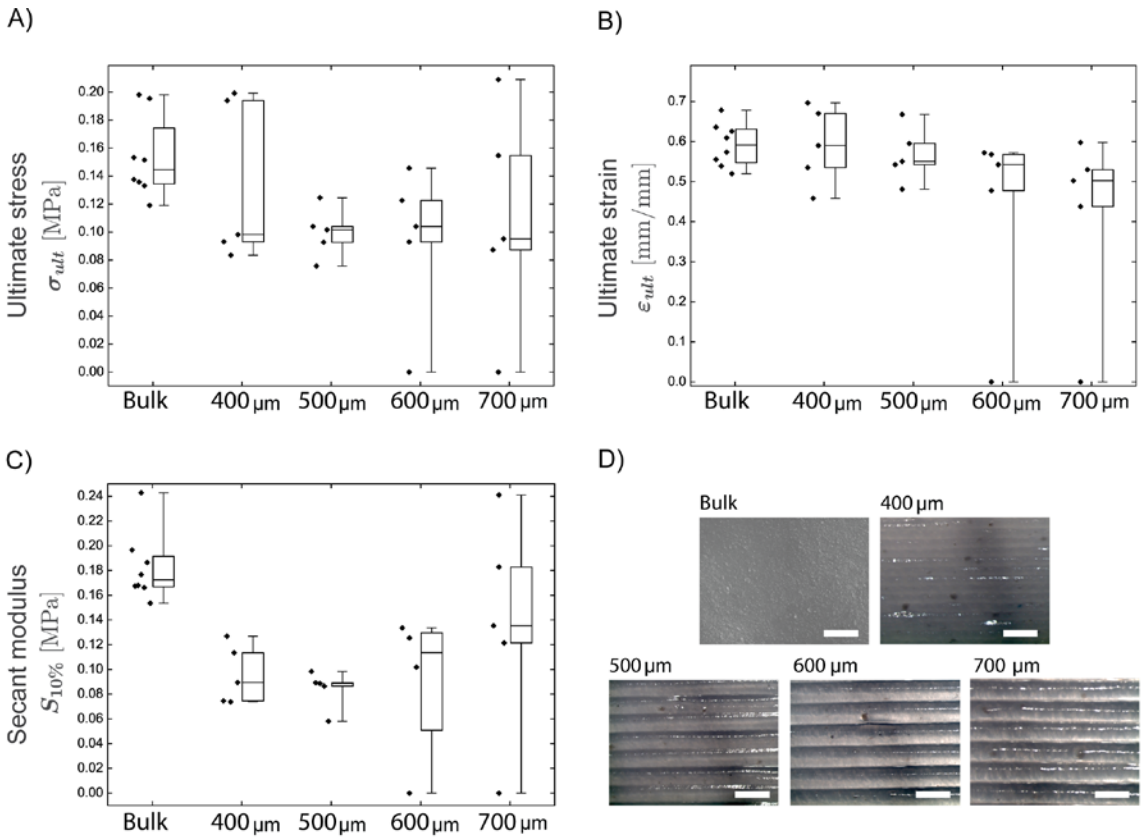

Figure 2. With increasing line spacing, there is an increased probability of defects in line-line adhesion in comparison to cast samples (bulk). A) Ultimate stress (Cauchy), B) ultimate strain

(local) and C) secant modulus (<10%) illustrate how probability of structural defects due to the printing process increased with the increasing line spacing. Each point represents a tensile specimen at failure and the values are represented also by boxplots where 50% of the values are in the box, middle line is the mean and tails represent the highest and the lowest values. The microscopy image for each line spacing shows the change in surface topography D).

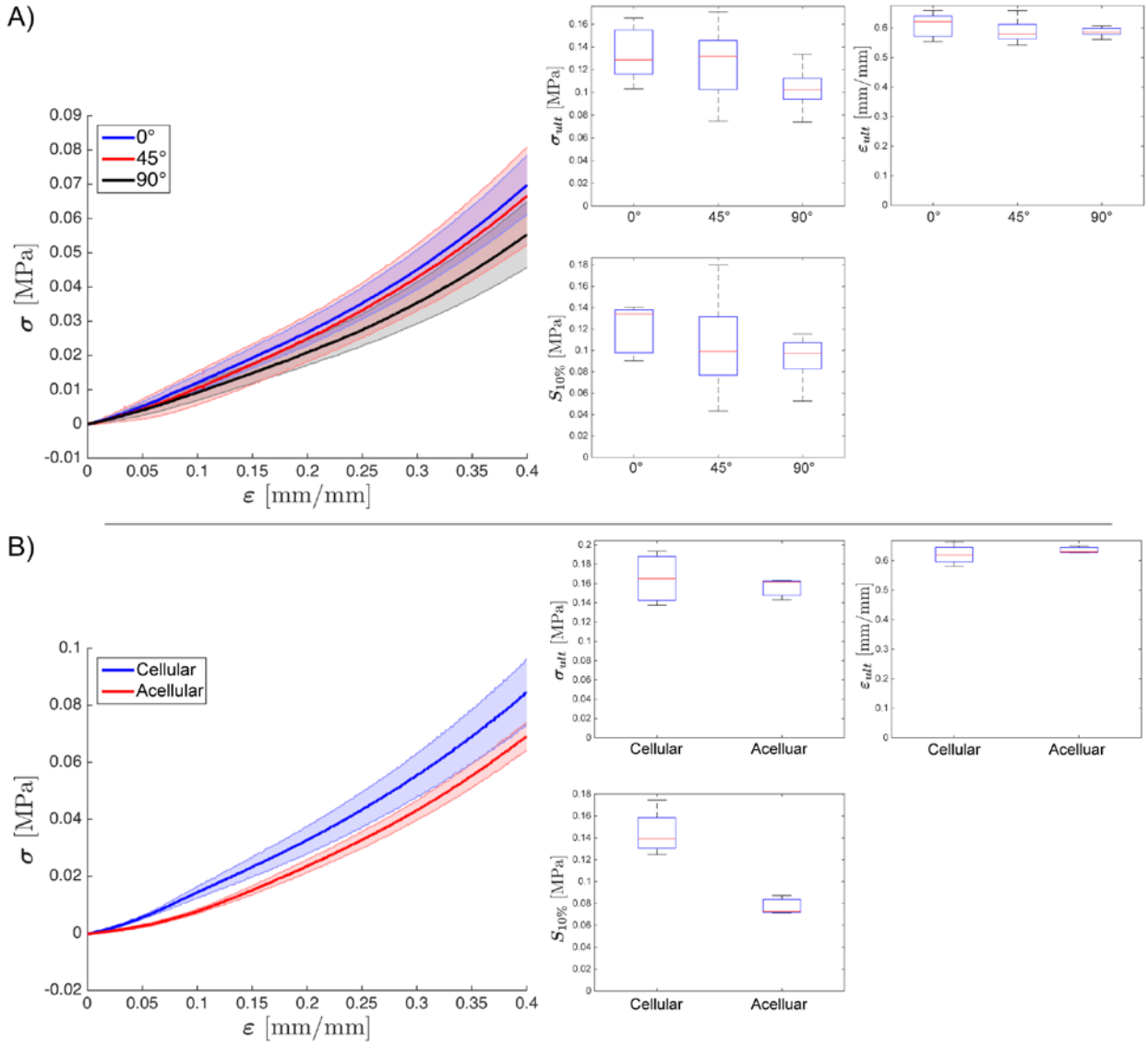

Figure 3. Tensile measurements of specimens with varying printing direction A) and comparison of cellular and acellular specimens B). The dumbbell specimens were printed in longitudinal (0°),

transverse (90°) or diagonal (45°) orientations with respect to the tensile direction. No significant differences were observed in ultimate stress (Cauchy), ultimate strain (local) or secant modulus (<10%) as a function of the printing direction. Furthermore, there was no significant differences in ultimate stress and strain when tensile properties of cell laden and acellular specimens were measured ($6x10^6$ cells/ml, ~1% v/v) while a significant difference in secant modulus was observed. The shaded regions of the stress-strain curve represent standard deviation (n=5).

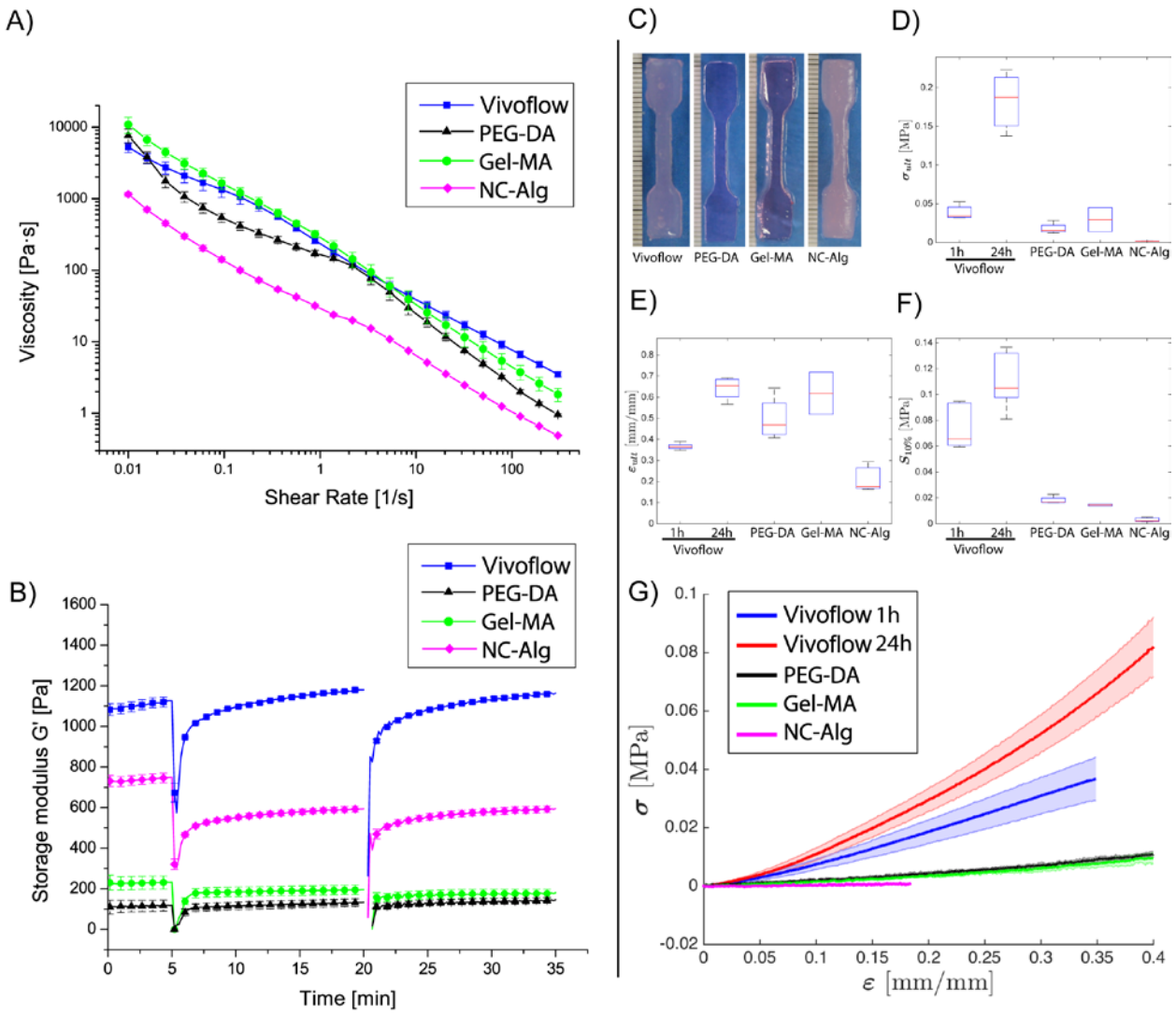

Figure 4. Comparison of rheological properties (A-B) and mechanical testing (C-G) of three commercial bioinks and Vivoflow. Shear thinning behavior was observed in all the bioink

compositions (PEG-DA, Gel-MA, NC-Alg) A) and shear recovery curves for all the bioinks suggested high levels of recovery (> 79%) B). Mechanical properties of tensile specimens C) with ultimate stress (Cauchy) D), ultimate strain (local) E), secant modulus (< 10%) F), and average stress-strain curves for each bioink G) are shown. Error bars (D-F) and shaded regions (G) represent standard deviation. Each condition was tested with minimum of n=3 in rheology and n=4 in tensile testing.

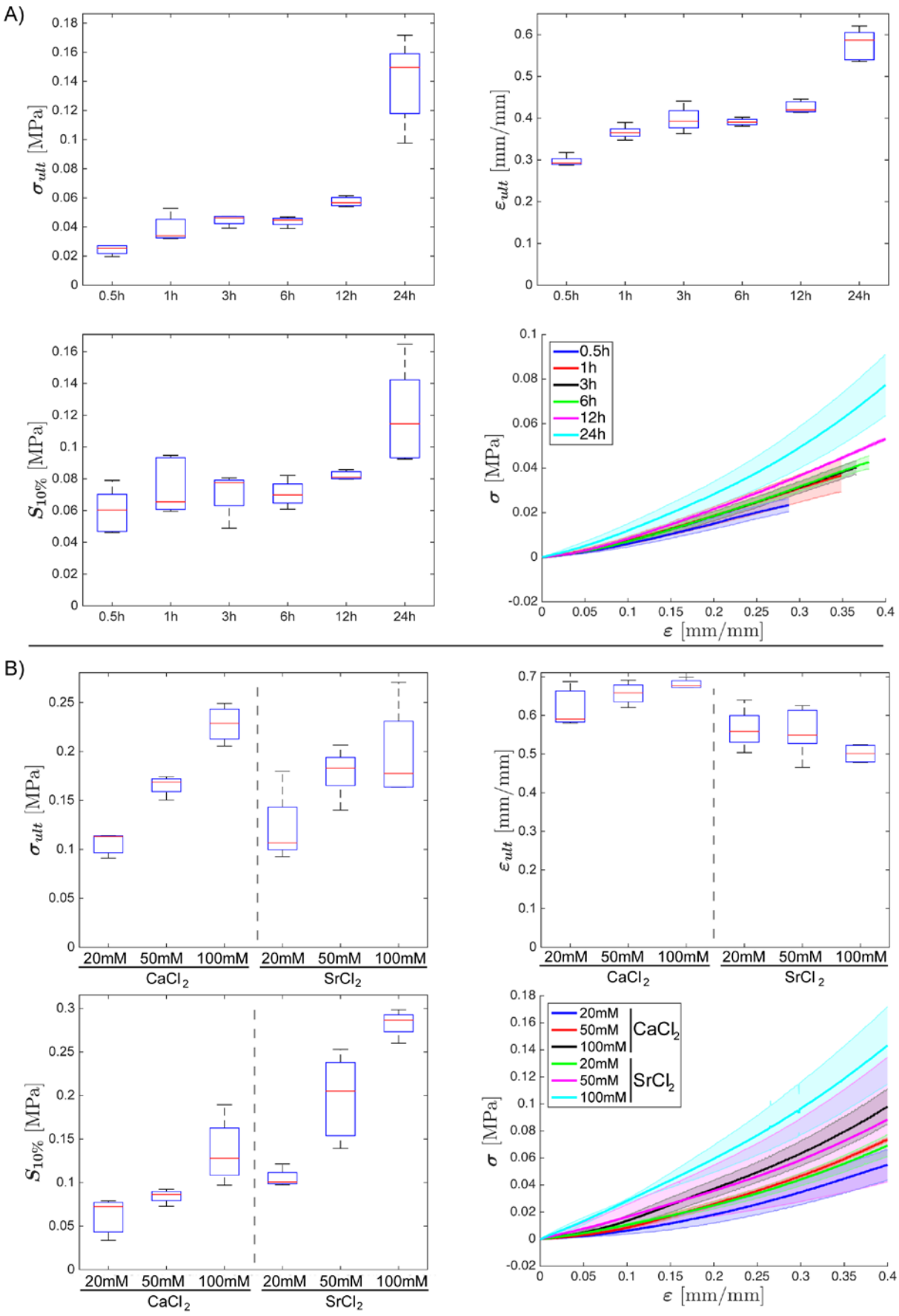
A)
σ_{ult} [MPa]
ε_{ult} [mm/mm]
$S_{10\%}$ [MPa]
σ [MPa]
ε [mm/mm]
0.5h
1h
3h
6h
12h
24h
B)
σ_{ult} [MPa]
ε_{ult} [mm/mm]
$S_{10\%}$ [MPa]
σ [MPa]
ε [mm/mm]
20mM
50mM
100mM
$CaCl_2$
$SrCl_2$

Figure 5. Mechanical properties of the Vivoflow printed grafts are tunable by crosslinking time A) and concentration and cation source B). The mechanical properties from lowest to highest were achieved between the crosslinking conditions 20mM $SrCl_2$, 0.5h and 100mM $SrCl_2$, 24h. The mechanical properties can be tuned after the bioprinting process which allows more cell specific approaches. The shaded regions in the stress-strain curve represent standard deviation. Each condition was tested with five samples (n=5). Ultimate stress (Cauchy), ultimate strain (local) and secant modulus (<10%) are represented.

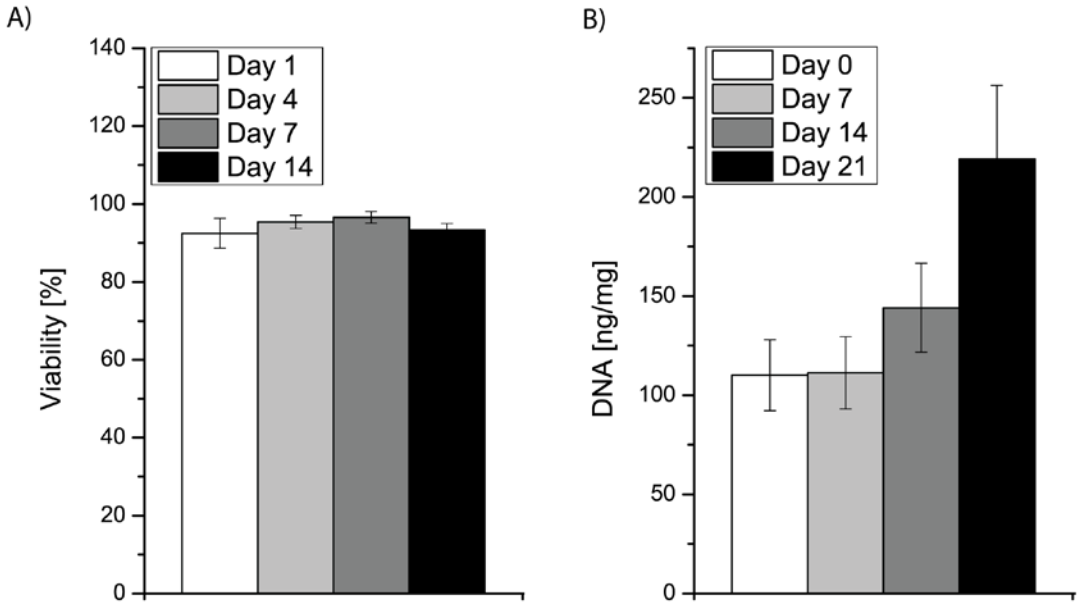

Figure 6. Biocompatibility assays performed for Vivoflow printed scaffolds. Viability of the embedded cells A) and DNA quantification as a measure of proliferation B). The error bars represent the standard deviation and each condition was tested with n=8 and n=6, respectively.